Structure formation in a conserved mass model of a set of individuals interacting with attractive and repulsive forces

Sergio E. Mangioni ●,* Matías G. dell'Erba ●, and Bruno Combi ●
IFIMAR (Universidad Nacional de Mar del Plata and CONICET), Deán Funes 3350, B7602AYL Mar del Plata, Argentina

We study a set of interacting individuals that conserve their total mass. In order to describe its dynamics we resort to mesoscopic equations of reaction diffusion including currents driven by attractive and repulsive forces. For the mass conservation we consider a linear response parameter that maintains the mass in the vicinity of a optimal value which is determined by the set. We use the reach and intensity of repulsive forces as control parameters. When sweeping a wide range of parameter space we find a great diversity of localized structures, stationary as well as other ones with cyclical and chaotic dynamics. We compare our results with real situations.

I. INTRODUCTION

Many natural or artificial systems, by being considered as a group of interacting individuals, subject to a nonlinear potential and affected by a random movement (temperature) driving its diffusion, can be modeled by means of mesoscopic equations of a reaction-diffusion type. Research about it has resulted in the formation of patterns and localized structures [1–10]. For some of these results, the attractive (medium-reach) forces between individuals played a relevant role. In these studies, explicitly or implicitly, repulsive forces of very short reach were also contemplated, but with a negligible effect compared with the attractive forces (just imposing a maximum limit on the density of individuals) [1–6].

However, works resorting to individual-based modeling in order to describe the collective movement in dynamical population have emphasized not only the importance of the medium-reach attractive forces (in order to avoid dispersion, thus promoting aggregation as a strategy of defense against predators [11,12]), but also that of the repulsive force, of shorter reach, in order to avoid collisions and overcrowding [13–19].

We believe it is necessary to develop an exhaustive study using mesoscopic equations of the reaction-diffusion type that, in addition to the effect of attractive forces, gives a relevant role to the repulsive forces.

From another perspective, the aforementioned mesoscopic models resort to a nonlinearity that in general aims to describe births, deaths, and effects of the environment, which may justify the fact that the mass (number of individuals) is not preserved during the dynamics that drives the system toward the steady state. This fact can be debatable in many real situations, for example, if the object of study is a group of individuals that obeys a collective dynamics. In this case, it is expected that a situation of stability requires that the mass of individuals remain constant during such dynamics. However,

the reality is that for no population does the mass remain exactly constant. Even if it is stable, there are always temporary variations around a given value of its average mass [20,21].

Following this line of thought, it would be expected that for a group of individuals whose subsistence depends on sustaining their mass within the range of a given optimal value [22], it provides some mechanism to achieve that purpose. A simple way to model it can be identifying linear response parameters to the variations of the mass, whose response ensures the recovery of its optimal value and, consequently, the subsistence of the whole.

Here we elaborate an illustrative one-dimensional model contemplating all these considerations, with the aim of revealing the possible stationary (forms of self-organization) and/or dynamics (cyclical or chaotic behavior) structural responses that a system with these characteristics could offer. Then we solve numerically the equations that describe its dynamics and compare the results with possible real situations. Finally, we focus on a type of stationary solution that we call localized patterns, place them in a context of reality, and characterize them through a spectral analysis.

Next we describe the model, show our results, place them in a natural context, and finally present our brief conclusions.

II. MODEL

A one-dimensional model of typical reaction diffusion can be described by

$$\partial_t u = F(u) + D\,\partial_{xx}u, \tag{1}$$

where $u(x)$, is a continuous function representing the individuals' density for a given position x, $F(u)$ (usually a nonlinear function) defines the behavior of the system, and D is the diffusion coefficient. This description has its limits. In order to conceive them, we consider dividing the space into cells whose size is large enough to include a large number of individuals, but much smaller than the characteristic size of the inhomogeneity that is intended to be described. In this

* smangio@mdp.edu.ar

014212-1

framework, u expresses the number of individuals per cell and x the location of the cell.

In particular, we consider studying a bistable system (with two possible stationary homogeneous solutions), so we propose

$$F(u) = A(u - \beta)(\alpha - u)(u - \gamma). \qquad (2)$$

This system accepts propagation fronts as solutions [23], but not localized structures or any other structure with dynamics. If $\beta < \alpha < \gamma$, such fronts evolve towards the stationary states β or γ, depending on which of the two is the most stable state. Then α is the threshold state (unstable) that separates the two attraction basins.

As already mentioned, we consider a population of interacting individuals. Depending on the distance between individuals, these repel or attract each other [13–19]. Attractive forces between particles adsorbed on a surface have already been incorporated into Eq. (1). This was carried out using a medium field technique that considers a current driven by the negative gradient of an average attraction force field $U^{[u]}(x)$. This field is constructed by adding up the potential due to the attraction between a "witness" particle, located at the point x, and all the particles located up to a certain distance r_a, which we call the reach of attractive forces [1–3,24]. Later a similar technique was applied to describe the gregarious instinct [4–6], a behavior that many species use to defend themselves from predators or improve access to food and foraging [11,12]. Then it was shown that the attractive forces between individuals (gregarious instinct) give rise to the formation and stabilization of simple structures and fronts connecting patterns. In those works [4–6], r_a was considered much greater than the reach of possible repulsive forces (r_r), a situation in which the effect of such forces on the dynamics that leads to the formation of patterns is negligible.

For some years now it has been emphasized that repulsive forces can be fundamental to define the behavior of populations [13–19]. Accepting that for most real situations the reach of attractive forces is greater, although not much greater, than the reach of repulsive forces, we believe it necessary to study more thoroughly its effect on the formation of structures and their dynamics.

We now, using the technique referred above, incorporate both effects into Eq. (1), that of the attractive and repulsive forces.

First, we write the average force field $U^{[u]}(x)$ caused by the interaction between individuals as

$$U^{[u]}(x) = U_a^{[u]}(x) + U_r^{[u]}(x),$$

where the subscripts a and r indicate attraction and repulsion, respectively. Then we write the average attracting (subscript a) and repelling (subscript r) force fields as

$$U_{a/r}^{[u]}(x) = I_{a/r} \int dx' f_{a/r}(|x' - x|) u(x').$$

Here $I_{a/r} f_{a/r}(|x' - x|)$ represents the attractive (subscript a) and repulsive (subscript r) potential (which is negative for attractive force and positive for repulsive force) between individuals separated by a distance $|x' - x|$, where $I_{a/r}$ is the corresponding intensity. Given the average character of both force fields, the details of their forms are irrelevant, therefore,

looking to shorten the times of the numerical calculation and considering $f_{a/r}$ normalized to 1, we choose a square shape, namely, $f_a(x) = \frac{-1}{2(r_a - r_r)}$ for $r_r \leqslant |x| \leqslant r_a$ and $f_r(x) = \frac{1}{2(r_r - r_m)}$ for $r_m \leqslant |x| < r_r$, where r_m indicates the minimum possible proximity between individuals, which limits their density to a value u_m. Of course, $f_{a/r}(x) = 0$ outside those limits.

The negative gradients of both average force fields drive currents: while the average attracting force fields tend to agglutinate the individuals, the average repelling force fields tend to disperse them. These currents would be proportional to $u(u_m - u)$, since the greater the density of individuals, the larger the current will be, and the greater the free space to circulate, the greater will be the current. However, we assume that there is an optimum density $u_o < u_m$ that conditions such currents so that they are proportional to $u(u_o - u)$. This means that the currents can change sign if such an optimum density is exceeded. In other words, the optimal density imposes a threshold for a drastic change in system behavior. Redefining u as $\frac{u}{u_o}$ and assimilating u_o in the system constants, we can replace $u(u_o - u)$ with $u(1 - u)$.

Later we will see that within a wide range of parameter values that we explore, our model produces structures such that $u(x) \leqslant 1$ for any x value (structures that we call normal). But, within the same range of parameters, our model also produces structures such that $u(x) > 1$ for short intervals $\delta x \sim r_r$ (which we call abnormal). This means that for this case, the model considers that when individuals pile up too much, the repulsive forces act like being attractive (the current agglutinates individuals instead of disperses them). The same phenomenon, but opposite, is also true for attractive forces, but since they act in a medium range and $u(x) > 1$ for short intervals $\delta x \sim r_r$, the corresponding effect is not very noticeable.

This situation makes us think of other one, when the nuclear forces dominate over the electric forces: if the distance between protons exceeds the radius of the atomic nucleus, the protons repel, but when this is lower than that radius, they attract. This effect of the model is harder to fit in a real physical or biological context. It expresses a kind of change of bond between individuals, which occurs when its average distance is shortened beyond a certain threshold. Since it does not seem unreal to consider individuals who respond to this rule (at least, we can think that this could mean a response of the species to overpopulation, predation, or a random fluctuation, or visualize artificially designed individuals that respond to that rule), and, given the surprising diversity of results obtained in this regard, we decided to include them in this report, but showing only some structures and dynamics, postponing a detailed study for later.

Considering the above arguments, we write the currents driven by the interactions between individuals as

$$J_{a/r}(x) = \varepsilon_{a/r} \, u(1 - u) \, \partial_x U_{a/r},$$

where $\varepsilon_{a/r}$ represents the respective interaction intensities weighted with the energy of movement (if the individuals were particles adsorbed on a surface, this energy would be kT, where k is the Boltzmann constant and T the temperature [1–3,24]).

We will use ε_r and r_r as our control parameters. Then the total current, including the diffusion, is

$$J_T(x) = -\partial_x u + J_a(x) + J_r(x). \tag{3}$$

In order to write this current, we have redefined $F(u)$ as $F(u)/A$ and rescaled t by A and x by $L_{\mathrm{diff}} = \sqrt{\frac{D}{A}}$ (diffusion length).

Therefore, for the model so far defined, the equation that governs the dynamics of the set of individuals that are attracted each other to medium distances and repel each other to short distances is written as

$$\dot{u} = F(u) - \partial_x J_T(x). \tag{4}$$

This model does not serve to describe a set of individuals whose number or mass is conserved. Next, we consider that there is an optimal mass for the survival of the set and a linear response mechanism that holds the mass in the vicinity of that value.

We choose the threshold (α) as the linear response parameter, which will change so that at each stage of the evolution of the system, the mass tends to remain approximately constant (around its optimal value). To build such a mechanism we write the mass of the system for a given time t_0:

$$m(t_0) = \int u(x, t_0) \, dx. \tag{5}$$

Then considering that for the time $t_0 + \delta t$, there will be produced a δu, we can write the mass for the time $t_0 + \delta t$ as

$$m(t_0 + \delta t) = \int u(x, t_0 + \delta t) \, dx \cong m(t_0) + \int \delta u \, dx. \tag{6}$$

Now, we consider that δu is produced not only by Eq. (4), but also by a correction $\delta\alpha$ whose objective is to recover the value of the mass corresponding to time t_0. Therefore,

$$\delta u = \left[F(u) + \frac{\delta F(u)}{\delta\alpha}\delta\alpha - \partial_x J_T(x) \right] \delta t. \tag{7}$$

Then for the mass recovering its value of time t_0 we must determine

$$\int \delta u \, dx = \int \left[F(u) + \frac{\delta F(u)}{\delta\alpha}\delta\alpha - \partial_x J_T(x) \right] \delta t \, dx = 0. \tag{8}$$

Considering that the current is null in $x = \mp\infty$, the current flow does not contribute to modify the mass, so Eq. (8) is reduced to

$$\int \left[F(u) + \frac{\delta F(u)}{\delta\alpha}\delta\alpha \right] dx = 0. \tag{9}$$

Thus, the linear response of the system to hold the mass around its optimal value, in each stage δt, is calculated as

$$\alpha(t + \delta t) = \alpha(t) + \delta\alpha = \alpha(t) - \frac{\int F(u) \, dx}{\int \frac{\delta F(u)}{\delta\alpha} \, dx}. \tag{10}$$

In summary, the dynamics of the system is determined by both Eq. (4) that in each stage δt modifies u and Eq. (10) that at each stage δt modifies α.

From a mathematical point of view, this mechanism can be applied to any parameter that characterizes the model; we choose α because it is the one that defines the stability of the

other two solutions and through its control the system can be converted to monostable, choosing which of the two solutions will remain.

In the context of natural populations, our view is that the mechanism represents the genetic or acquired response of a system that, by natural selection, it learned to conserve its average mass by controlling the value of that parameter. The information handled by this parameter can be related to births and deaths, with migrations toward places of higher or lower foraging or predation, with the incorporation or expulsion of individuals to or from the system, etc. We can also imagine artificial contexts, in which the conserved parameter is not necessarily the mass, which opens a panorama that can lead to robotics [25–27]).

If we think of a group of individuals whose subsistence depends on their cohesion and conservation of their average number, the nonlinearity added to the mechanism of linear response and attractive forces would constitute a synergistic response to the attempts of the environment to break that cohesion and/or change their number. On the other hand, repulsive forces have the function of signaling an optimal living space for the proper functioning of each individual. Regarding the solutions for which $u(x) > 1$ within a short interval $\delta x \sim r_r$ (abnormal), one can think of a readaptation to the overpopulation or predation or in artificially constructed individuals.

In general terms, we here propose a homogenously bistable system model, mathematically simple, that includes attractive and repulsive forces between individuals, and a linear response mechanism to maintain the bounded mass in the vicinity of an given optimal value, all this with the objective of exploring its capacity to generate various structures as possible responses to the eventualities posed by its environment.

III. RESULTS

In order to numerically resolve the dynamics defined by Eqs. (4) and (10), we proceed to do a spatial discretization in a regular one-dimensional lattice composed of 28 800 sites with spacing $\delta x = 6.25 \times 10^{-3}$ and time step $\delta t = 6.25 \times 10^{-6}$ (for the most sensitive situations, we use $\delta t = 6.25 \times 10^{-7}$), i.e., $u(x_i) \longrightarrow u_i$, with i the cell index. The numerical scheme used in the simulations is the method of finite differences. We ensure the numerical convergence applying the criterion $\frac{dt}{dx^2} < 0.16$. Considering that $\partial_x^2 u \longrightarrow \frac{1}{\delta x^2} \sum_j (u_j - u_i)$ (one dimension), where the sum is over the nearest neighbors, the discretized version of Eq. (4) is written as

$$\frac{\delta u_i}{\delta t} = F(u_i) + \frac{1}{\delta x^2}\sum_j (u_j - u_i) + \frac{1}{2\delta x}\left[\delta J_a^i + \delta J_r^i \right], \tag{11}$$

where

$$\delta J_a^i = u_{i+1}(1 - u_{i+1})(U_a^{i+2} - U_a^i)$$
$$- u_{i-1}(1 - u_{i-1})(U_a^i - U_a^{i-2}),$$
$$\delta J_r^i = u_{i+1}(1 - u_{i+1})(U_r^{i+2} - U_r^i)$$
$$- u_{i-1}(1 - u_{i-1})(U_r^i - U_r^{i-2}),$$

and

$$U_{a/r}^i = \mp \frac{\varepsilon_{a/r}}{2(r_{a/r} - r_{r/m})} \sum_{j_{a/r}} \frac{u_{i+j_{a/r}+1} + u_{i+j_{a/r}}}{2},$$

where $j_{a/r}$ indicates that the sum is over the attractive or repulsive force's reach, respectively.

Then the discretized version of Eq. (10) is written as

$$\alpha(t + \delta t) = \alpha(t) - \frac{\sum_i F(u_i)}{\sum_i (u_i - \beta)(u_i - \gamma)}.$$

In order to ensure zero flow in the border we used as boundary conditions $\partial_x u = 0$. Since the force field $U_{a/r}^i$ depends on u_i with i varying from $i \pm 1$ to $\pm i_{r_{a/r}}$, we apply this condition from the system's right or left border until the cell $\pm i_{r_{a/r}}$.

As mentioned before, we choose as control parameters those that characterize the repulsive forces (ε_r and r_r), and we assign values to the rest of the parameters based on already known results [5,6]. So, for all our results, $\beta = 10^{-4}$, $\gamma = 0.9$, $\varepsilon_a = 12$, and $r_a = 1$. Then we vary r_r from 0.1 to 0.9 and ε_r from 1 to 96.

We started by launching the system from an approximately rectangular profile built with hyperbolic tangents, sweeping the parameter space in the aforementioned range. Except for the value of the initial mass, the result was independent of the particular detail of this profile. For all the cases reported in this paper, we use an initial mass $m = 320$, and it is practically a rectangle of sides $\Delta x = 800$ and $\Delta u = 0.4$. Although the initial mass value defines the optimum mass value, it is not equal to the latter. In a short transient, the system determines the optimal mass. For the initial mass value that we use, the optimum mass has always a small correction $|\delta m_c| < 0.3$, which is added to 1283. Once the system determines the optimum mass ($m_o = 1283 + \delta m_c$), the same remains constant provided that the solutions found are stationary (a fact corroborated up to the computer's accuracy limit). The same goes for the linear response parameter α. By varying the control parameters, the small correction δm_c changes slightly, but its absolute value is always less than 0.3. For solutions with dynamics, δm_c varies slightly with time, meaning oscillations of m_o with an amplitude of the order of 10^{-2} at most (relative amplitude of the mass oscillations: $\lesssim 10^{-5}$). When we test with other values of the initial mass, we do not observe significant qualitative changes in our results. That is why we focus on a single initial mass value.

In order to optimize the solution search process, every time an atypical structure stabilized, we went back to sweeping the parameter space, but initiating the system from that atypical structure. In all cases the system held the mass around its optimal value ($1283 + \delta m_c$). Thus we went through that space several times, each time starting the system from a different profile. Using this simple but laborious strategy we found diverse structures with stationary form and dynamic structures showing cyclical or chaotic behavior. The latter are like those stationary or similar, but varying with time, moving, and deforming. Although this behavior was observed for both types of structures (normal and abnormal), it is much more abundant and forceful for abnormal structures than for normal ones. Except for cyclic or chaotic cases, the normal structures were always symmetrical, while the abnormal ones, depending on
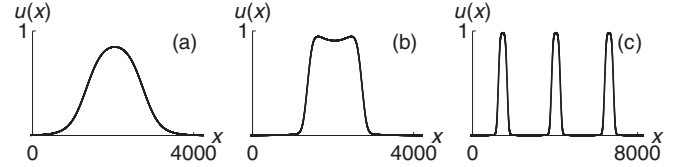

FIG. 1. Simple localized structures (normal): (a) $r_r = 0.3$ and $\varepsilon_r = 10$; (b) $r_r = 0.3$ and $\varepsilon_r = 3$; (c) $r_r = 0.2$ and $\varepsilon_r = 1$.

the values of the parameters, for some cases were symmetrical; for others they were asymmetric, and even, depending on the initial condition, for the same set of parameter values, we obtained symmetric and asymmetric solutions. Whenever we tried, we were able to find the antisymmetric solution (as seen in a mirror) of a previously obtained asymmetric solution. Although we did not do it for all cases (we found many asymmetric solutions), we did it enough times to convince ourselves that this was the rule.

A fact to be highlighted is that, while the symmetrical stationary solutions always resulted in zero speed, the stationary asymmetric solutions resulted in a constant speed, whose direction is defined by the asymmetry of the structure. In fact, the more asymmetric, the faster they moved (of course, the corresponding antisymmetric solutions always moved in the opposite direction). Consistent with the behavior described above, the dynamic structures showed a speed that changes with their shape. Since the equations are spatially symmetric, the stabilization of asymmetric solutions could indicate symmetry breaking; however, because asymmetric structures move, we tend to believe that such asymmetry could be compensated by the current associated with said movement: the asymmetry drives the current, and the latter sustains such asymmetry. In fact, this could be the thread by which to look for an explanation for dynamic solutions. Inhomogeneous currents that vary over time are driven by asymmetries (spatial variations in density) whose inhomogeneities generate variations in time of such currents. Temporal and spatial variations of one and the other mutually feed back. We will postpone this discussion for another paper; we think that the subject requires a more comprehensive work. Next, although we show some representative examples selected from the great variety of solutions obtained, we will focus on those that we named before as normals.

We classify the normal forms into smooth localized structures (SLSs) and localized patterns (LPs: a localized envelope modulating a pattern). In Fig. 1 we show examples of SLSs, in Fig. 2 we show examples of LPs, and in Fig. 3 we show same examples of abnormal forms.

The formation of patterns and localized structures in reaction-diffusion models that include attractive forces between individuals should not be surprising. Opposing the diffusion process (which homogenizes), attractive forces (binders) destabilize homogeneous solutions and give rise to the formation of patterns and smooth localized structures [5]. The novelty here is that, by adding the effect of short-range repulsive forces and a mechanism that conserves the mass of the system, localized patterns emerge. Later we will see that the spatial period of these localized patterns grows with the reach of the repulsive forces, a fact that highlights the effect
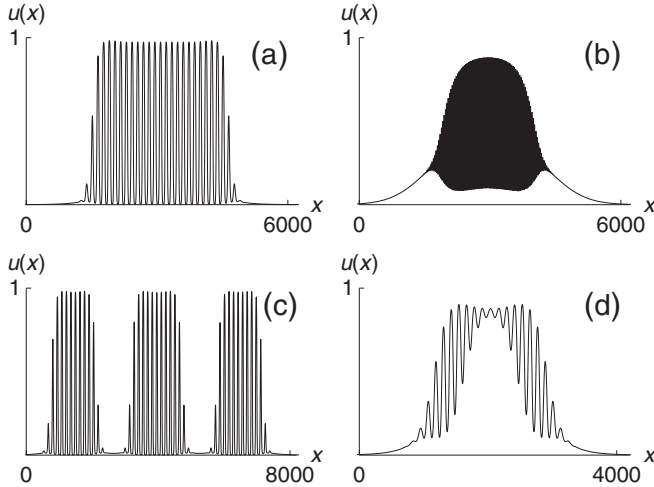
FIG. 2. Localized patterns (normal): (a) $r_r = 0.6$ and $\varepsilon_r = 5$; (b) $r_r = 0.15$ and $\varepsilon_r = 20$; (c) $r_r = 0.7$ and $\varepsilon_r = 7$; (d) $r_r = 0.45$ and $\varepsilon_r = 10$.

of such forces on the conformation of the pattern within the envelope.

Looking at Fig. 2 we notice that most of the localized patterns have a very high spatial frequency in relation to the width of their envelope. The global view gives the impression of evenly spaced discontinuous peaks. We make clear that all profiles are continuous. As an illustration of this, in Fig. 4 we show an enlargement of part of Fig. 2(b).

For stationary structures (forms with or without velocity that are sustained over time), after an initial transient (short in relation to the total observed time), both the mass and the linear-response parameter α are held at a constant value. But, differently, the cases of cyclic or chaotic behavior manifested through the curves of α versus t, which were correlated with corresponding changes in the forms of the structures. The variations in time of $\alpha(t)$ were also correlated with the variations of the mass of the system, but, while the relative variations of $\alpha(t)$ were remarkable, the relative variations of the mass were completely negligible. Comparing the corresponding quotients between the average sizes of the oscillation and the average values of the parameters in question, in all the observed cases we find that the relative variations of $\alpha(t)$
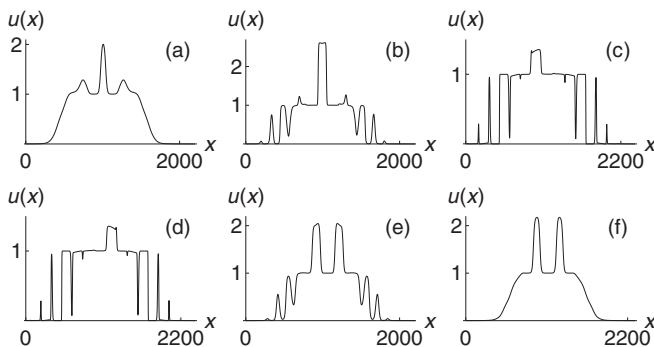

FIG. 3. Abnormal structures: (a) $r_r = 0.45$ and $\varepsilon_r = 3$; (b) $r_r = 0.7$ and $\varepsilon_r = 25$; (c) and (d) $r_r = 0.9$ and $\varepsilon_r = 80$; (e) $r_r = 0.7$ and $\varepsilon_r = 5$; (f) $r_r = 0.6$ and $\varepsilon_r = 3$.

FIG. 4. Localized patterns (normal). Enlargement of part of Fig. 2(b): $r_r = 0.15$ and $\varepsilon_r = 20$.

are several orders of magnitude larger than the corresponding variations of the mass. In this regard, we conclude that the linear response mechanism satisfies the intended objective: to maintain the mass of the system in the vicinity of an approximately constant average value.

In the following, we will show some examples among the many observed cyclic and chaotic cases: curves of $\alpha(t)$ accompanied by profiles samples illustrating such evolution (samples taken every certain time interval).

A. Cyclical or chaotic behavior

First, we illustrate the cyclical or chaotic behavior for normal patterned forms (localized patterns). These arise for small values of r_r and large values of ε_r (see figure captions to roughly locate the parameters domain and specific data). We did not find significant differences between the observed forms for different values of the parameters within the pertinent domain (see Fig. 14). Figure 5 shows the curves of α versus t corresponding to a cyclic and another chaotic case,
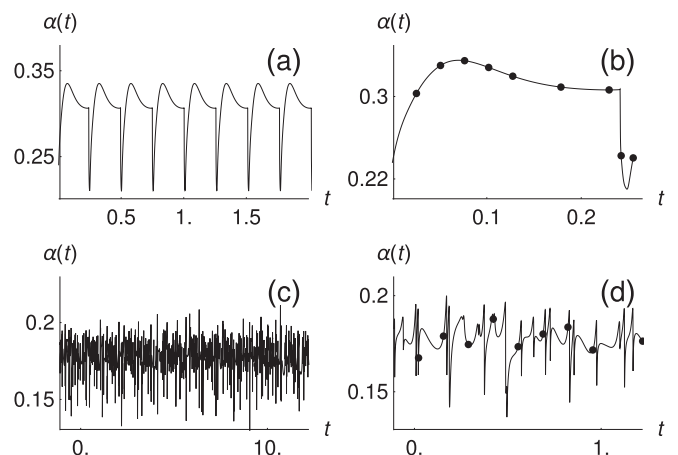

FIG. 5. Localized pattern (normal) case: $\alpha(t)$ curves. (a) $r_r = 0.4$ and $\varepsilon_r = 90$. (SCDS); (b) a previous case cycle [full circles indicate the sample times for profiles $u(x)$ we will show in Fig. 6]; (c) $r_r = 0.35$ and $\varepsilon_r = 60$. (CDS); and (d) previous case: focusing on a shorter time. $t = 10^7 \delta t$, where $\delta t = 6.25 \times 10^{-6}$.
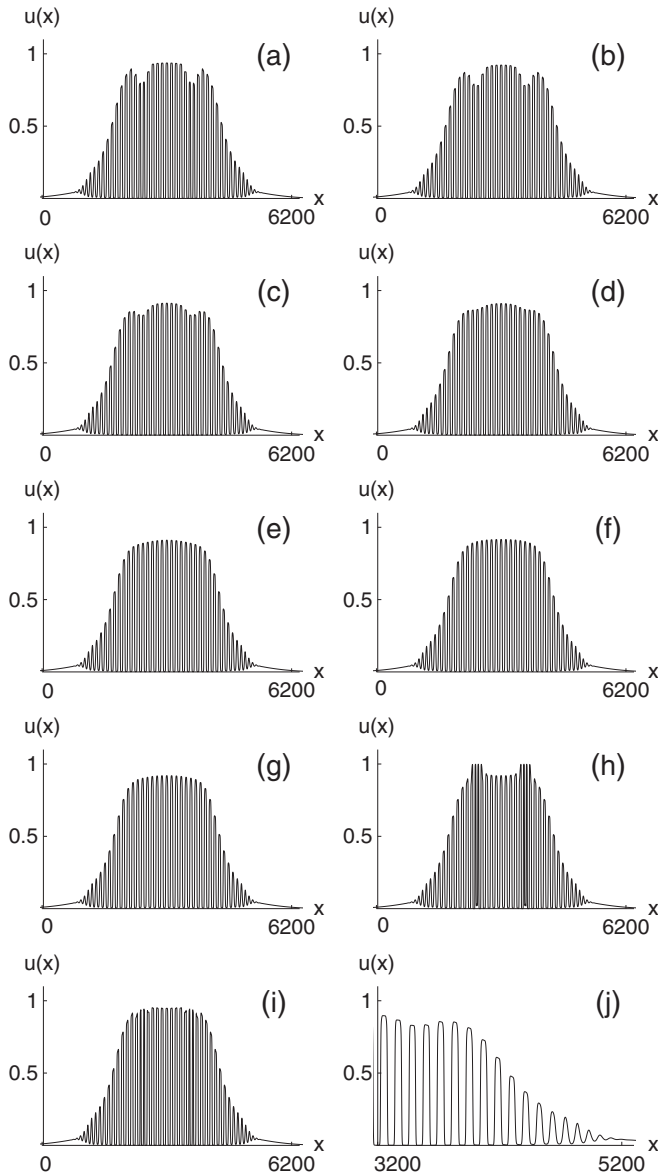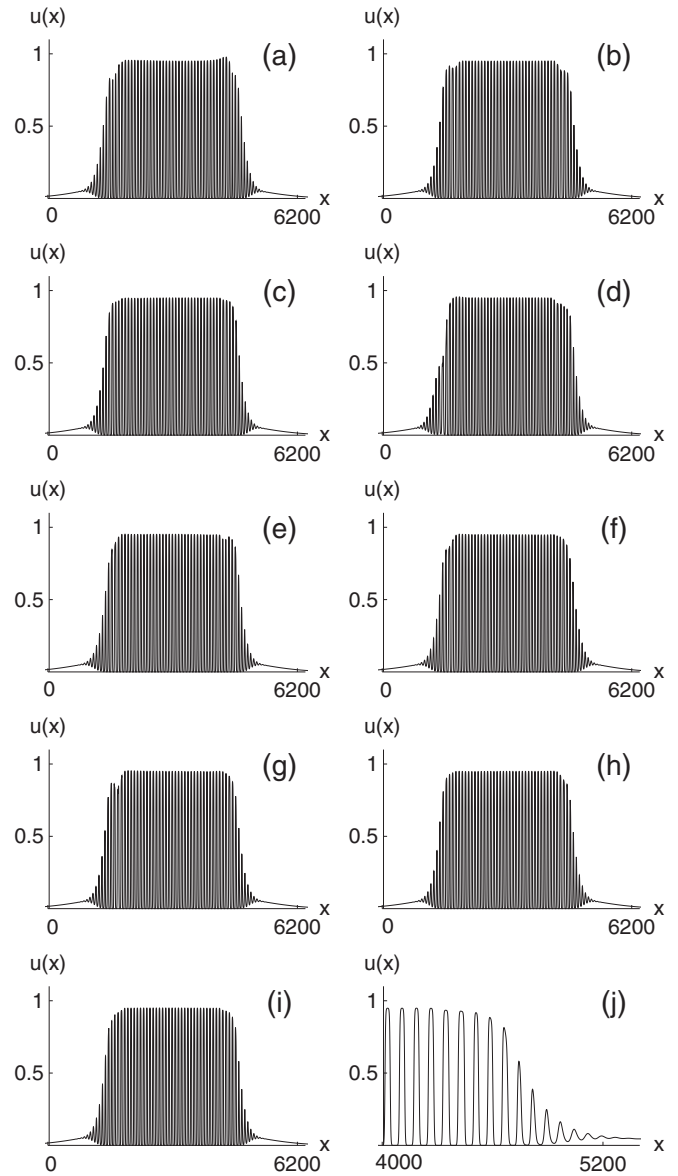
FIG. 6. Localized pattern (cyclic normal form) case: successive samples of profiles $u(x)$ corresponding to the case shown in Fig. 5(b). They were taken in same time and order indicated by the full circles. In order to better illustrate the localized patterns, we show in (j) an enlargement of part of (c).

FIG. 7. Localized pattern (chaotic normal form) case: successive samples of profiles $u(x)$ corresponding to the case shown in Fig. 5(d). They were taken in the same time and order indicated by the full circles. In order to better illustrate the localized patterns, we show in (j) an enlargement of part of (i).

which were calculated during a much longer time than the characteristic times observed in the dynamics. We also show the curves focusing on a short time interval to illustrate the detail (a period for the cyclic case). The points marked in these last curves allow us to identify the time values for which we show $u(x)$ in Figs. 6 (cyclic) and 7 (chaotic). We observe that $u(x)$ is a localized pattern, that is, a localized envelope modulating a pattern. We observe that the spatial period changes significantly with the control parameters but does not do so over time, while the localized envelope, in addition to varying significantly with control parameters, also does so over time. The changes of the localized envelope with t are evident for the cyclic case and barely perceptible for the chaotic case. We also note that such a difference in the

sensitivity of the envelope with respect to time is correlated with the difference in the range of variability of α, which is much smaller for the chaotic case than for the cyclic case. In summary, for normal forms the chaotic behavior consists of very small fluctuations of the envelope of the structure which are motivated by variations of the α parameter, that in turn are produced with the objective of conserving the mass around a given optimal value.

Next, although it is not a main topic of our article, we also show an example for abnormal cyclical dynamical structures and another for those that are chaotic. Figure 8(a) shows $\alpha(t)$ for an interval long enough to reveal the periodicity of the dynamics, and Fig. 8(b) shows one of the cycles in detail. The points indicate the sample times of the profiles shown in Fig. 9
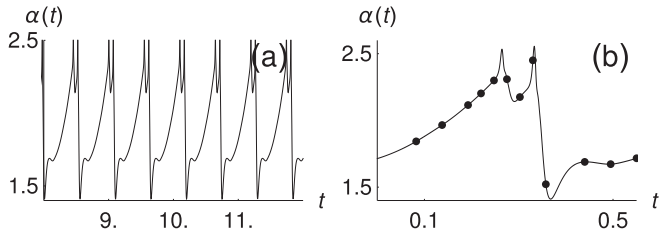
FIG. 8. Dynamic abnormal structures, an example illustrating the behavior observed in cyclical cases: $\alpha(t)$ curve. (a) $r_r = 0.63$ and $\varepsilon_r = 4$; (b) a previous case cycle [full circles indicate the sample times for profiles $u(x)$ we will show in the following figure]. $t = 10^7 \delta t$, where $\delta t = 6.25 \times 10^{-7}$.

(see figure captions to roughly locate the parameters domain and specific data). Figure 10 shows $\alpha(t)$ for a intermittent chaotic case (interspersed by short quasiperiodic intervals). It is evident that no global period is recorded in such a curve, which also indicates chaotic behavior. Figure 10(b) is a focalization over a much shorter time range, where we can see the details. Figure 11 displays samples of the successive profiles that emerge as time passes.

We note that for abnormal forms we also find completely chaotic cases, with curves $\alpha(t)$ such as those one shown in Fig. 5(c).

As in the case of localized patterns, some abnormal structures and some $\alpha(t)$ curves exhibit sharp peaks that suggest discontinuities. In this regard, we clarify that all our calculations have sufficient resolution to guarantee continuity in such cases. First, such as for localized patterns, an enlargement of

the suspected parts of such structures reveals a continuous curve. Second, in order to avoid large files, the points to construct the $\alpha(t)$ curves were taken every certain number of calculated points. For many of the cases in which we suspect discontinuity we increased the frequency of sample points, and thus we could observe that the suspected structures turned out always to be continuous, and, except for a few chaotic cases, we were also able to corroborate the continuity of the questioned $\alpha(t)$ curves. As an example, in order to illustrate these situations, we show the curves of $\alpha(t)$ for a periodic and another chaotic case. In Figs. 12 and 13 show the corresponding curves.

B. Phase diagrams for normal forms

We made maps using curves of ε_r versus r_r to locate domains of normal forms. This is shown in Fig. 14. The entire range of scanned control parameters is divided into two main domains. One domain that corresponds to stationary smooth

FIG. 10. Dynamic abnormal structures, an example illustrating the behavior observed in chaotic cases: $\alpha(t)$ curve. (a) $r_r = 0.35$ and $\varepsilon_r = 19$; (b) same as the previous case, but for a very much shorter time. $t = 10^7 \delta t$, where $\delta t = 6.25 \times 10^{-7}$.
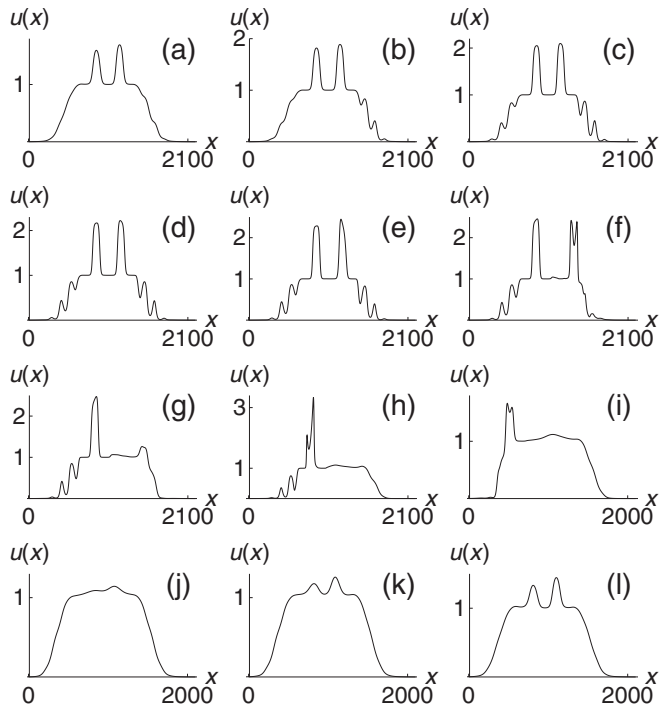

FIG. 9. Dynamic abnormal structures: successive samples of profiles $u(x)$ corresponding to the case shown in Fig. 8(b). They were taken in the same time, and order is indicated by the full circles.
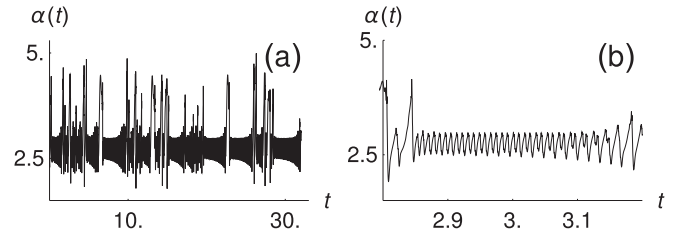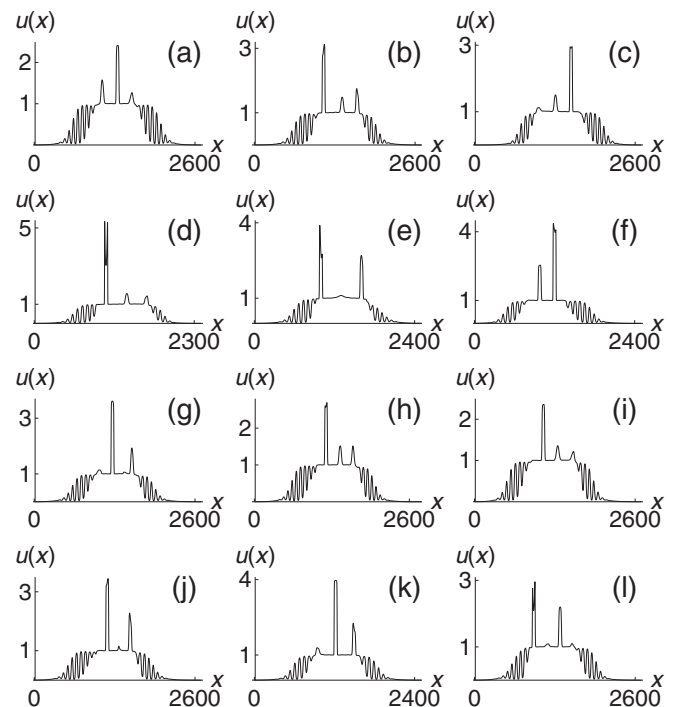

FIG. 11. Dynamic abnormal structures: successive samples of profiles $u(x)$ corresponding to the case shown in Fig. 10(c).
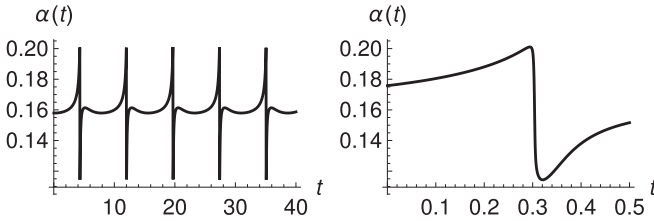
FIG. 12. Dynamic abnormal structures: an example of a periodic case in which the $\alpha(t)$ curve appears to be discontinuous, but an enlargement of the supposed discontinuity shows that it is not. (a) $\alpha(t)$ curve for $r_r = 0.35$ and $\varepsilon_r = 45$; (b) enlargement of an apparent discontinuity. $t = 10^7 \delta t$, where $\delta t = 6.25 \times 10^{-7}$.

localized structures (SLSs), roughly defined by the ranges of ε_r and r_r: [1, 20], [0.1, 0.65], and the other one, the rest of the parameters range explored, correspond to the (stationary and nonstationary) localized patterns (LPs), a range that in turn we divide into three domains: stationary (SLP), cyclical (WLP), and chaotic (FLP). On the line that limits both domains, the solutions are like that one displayed in Fig. 2(d), which describes an intermediate situation between a smooth localized structure and localized pattern. We notice that there is a small region (striped area in plot) of superposition of the two main domains, a fact that at least indicates bistability: depending on the shape of the excitation, the system can evolve to a smooth localized structure or a localized pattern. On the map, the cyclical dynamics regions is marked with the label WLP and the chaotic dynamics regions with the label FLP.

For the same range of previously scanned parameters, depending on the initial profile, abnormal solutions also emerge. We consider that, given the great diversity of these solutions, a map similar to the previous one is too convoluted and therefore not very illustrative.

We note that for each situation (defined by the values of the control parameters) there are several possible solutions. Thus, it is the initial profile that defines which of these solutions the system will select.

IV. MODEL RESULTS AND REALITY

What do these results tell us about a group of individuals with the capacity for self-organization? A group of living beings must feed and protect themselves from the attacks of the environment (predators, climatic variations, etc.) to
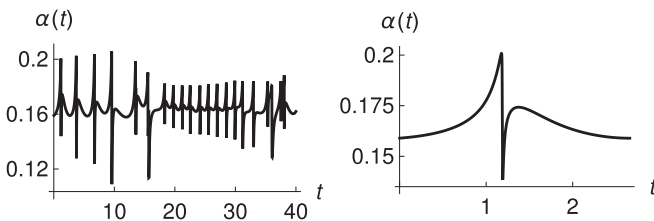

FIG. 13. Dynamic abnormal structures, An example of a chaotic case in which the $\alpha(t)$ curve appears to be discontinuous, but an enlargement of one of the supposed discontinuities shows that it is not. (a) $\alpha(t)$ curve for $r_r = 0.35$ and $\varepsilon_r = 50$; (b) enlargement of an apparent discontinuity. $t = 10^7 \delta t$, where $\delta t = 6.25 \times 10^{-7}$.
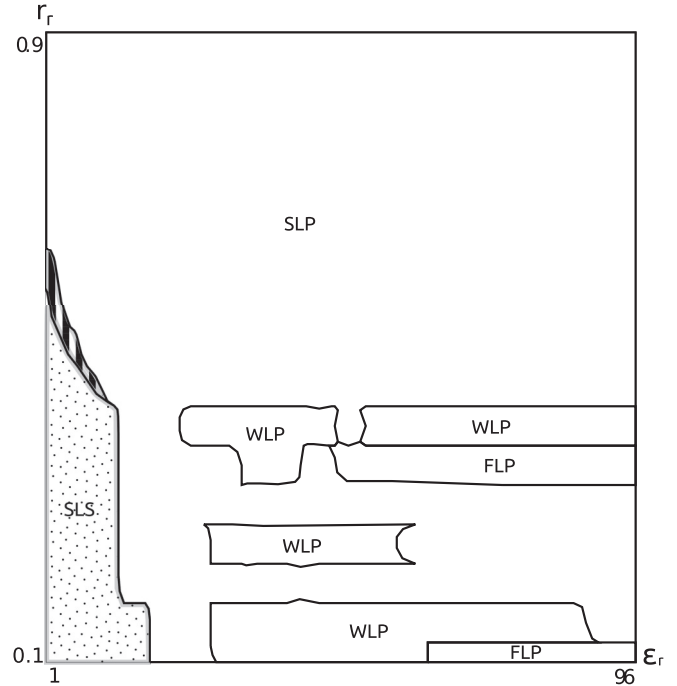

FIG. 14. Phase diagram for normal structures: punctuated area $\mapsto$ domain corresponding to stationary simple localized structures (SLSs), white area $\mapsto$ domain corresponding to (stationary -SLP-, periodic -WLP-, and chaotic -FLP-) localized patterns (LPs), and striped area $\mapsto$ overlap between both domains.

survive. Since the food is obtained from the environment, the larger the area of exposure, the better the foraging. Under this premise, individuals should be scattered throughout the environment. However, it is known that many living beings, from microorganisms [28–31] to mammals [11,32–34], including insects [18,35–40], birds [21,22,41], and fish [13–17], tend to aggregate and move together, a phenomenon that is usually referred to as gregarious or herd instinct or also collective movement. The reasons for aggregation are diverse; the most widespread is that of defense against predators, although they can also come together to create an appropriate climate for their biological and/or social functions, to execute foraging strategies, for more accurate navigation, or a combination of these factors. Therefore, there is a compromise between predation risk or other factors and foraging optimization. In this regard, we can consider several situations for which the solutions of our model are a good answer:

Situation A: there are no predators, a group temperature above that of the environment is required, and food is scarce. Answer A: smooth structure as shown in Fig. 1(c).

Situation B: there are a few predators, a group temperature above that of the environment is required, and the food is abundant. Answer B: smooth structure as shown in Fig. 1(a) or (b).

Situation C: There are many predators and a group temperature above that of the environment is required, but food is scarce. Answer C: localized pattern.

To solve case "A," since there is no danger of predator attacks, the group can expose a large area to the environment. Then, to solve case "B," when some predators are present,

the strategy to reduce the risk is to reduce the exposure area; furthermore, if food is abundant, a large exposure area is not necessary. Finally, case C is extreme, and therefore extreme measures are necessary and they are required: (1) a large area of exposure to access the food and (2) a small area of exposure against predators. Assuming that the food is much smaller than the predator (or depending on the case, individuals and food much smaller than a predator's mouth [42]), a localized pattern offers the appropriate response.

The self-organization of microorganisms in biofilms deserve a particular mention. Depending on the aggressiveness of their environment, bacteria in biofilms adopt different phenotypes to survive and procreate [43]. The rugose and smooth variants are two examples that have been known for many years [42]. Each phenotype has physical properties that distinguish it from the others: resistance to osmotic, acidic, oxidative, and biological stressors [44]. In particular, studies have shown that production of smooth and rugose variants is a defensive strategy adapted by *Vibrio cholerae* against predation by protozoan grazing [45], a major cause of bacterial mortality in natural aquatic habitats. In general, microorganisms change phenotype to increase population diversity and maximize evolutionary success. Variation between smooth and rugose phenotypes can be controlled by changing a nucleotide in a gene [46].

From another approach, the confinement of the cells, intrinsic to the biofilm growth mode, induces multiple physico-chemical gradients which can impact various biological functions. Such changes translate into different physico-chemical interactions [47–50]. Models that consider these interactions have resulted in the formation of both smooth and high-order structures [51,52]. Of particular interest to this paper are the ring and wrinkle patterns observed in biofilms [53–55], whose one-dimensional versions look very similar to our localized patterns and to some of our abnormal forms. Since the biofilm expansion on nutritious surfaces enhances nutrient uptake [56], the patterning (ring and wrinkle) is a way that may enhance its availability as an answer to scarcity [57].

In this paper, we reduce all interactions to short-range repulsive and medium-range attractive forces. If we, in addition, consider that interactions between bacteria in biofilms can drive their mobility [58] and that biofilm populations have limitations such as availability of nutrients in the immediate environment, the penetration of these nutrients into the biofilm, the elimination of residues, the desorption and death of bacteria, etc., all these phenomena leading to a stationary situation, we note that our one-dimensional model has all the necessary ingredients to outline a simplified description of the generic behavior of a biofilm.

In summary, the individuals that our model contemplates can be microorganisms, insects, birds, fish, or mammals, all of them with different response times, which are considered through the parameter A in Eq. (2). As a thought exercise, we can consider each such individual as a being that reacts automatically to the disturbances provoked by the environment. The set of disturbances $\mapsto$ possible reactions would be genetically "carved" by the history of the species. Then we consider that each of these automatic reactions involves two processes. Primary to them is the selection of the set

of values of the parameters that define their interaction (response state), which would be the same for all individuals, since such selection would determined by the disturbance. The other process is related to the choice of initial profile. If we include abnormal structures in this analysis, the multistability is ensured for all situations, and therefore the initial profile becomes relevant. The disturbance could generate a random movement, and then the final selection of the structure or response between the two, three, or four options, according to the degeneration of the response state, would also be random. But the most probable is that the disturbance implies a certain degree of order which would be partially transferred to the initial profile. Therefore, the structure or response would also be determined by the disturbance, since once the initial profile is determined, the basin of attraction corresponding to a given response is also determined.

Thus, this simple model, which we might consider a toy model, allows us to show that it is possible that a population, resorting to a mechanism of responses to environmental disturbances based on the manipulation of the reach and intensity of repulsive forces between individuals, would dispose of multiple options to define these responses.

V. SPECTRAL ANALYSIS

A. Localized patterns

We did Fourier transforms of the patterned solutions, for which we adapted a fast transform program (FFT) from Numerical Recipes [59]. In addition to the spatial frequency of the enveloped pattern (ν_e), we calculated what we call the center of frequencies and the dispersion around it. In other words, the localized pattern exposes a main frequency ν_e that can be calculated by measuring the distance between folds $\tau_e = 1/\nu_e$,
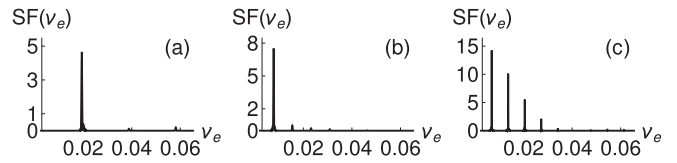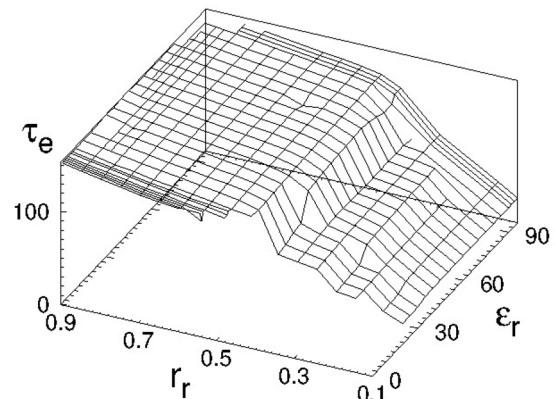
FIG. 15. Spectral function ($SF/10^5$) for three typical cases: (a) $r_r = 0.2$ and $\varepsilon_r = 50$; (b) $r_r = 0.5$ and $\varepsilon_r = 50$; (c) $r_r = 0.8$ and $\varepsilon_r = 50$.

FIG. 16. Special period τ_e (distance between folds) vs r_r and ε_r.

FIG. 17. Center of frequencies (ν_e^c) vs r_r and ε_r.

FIG. 19. Special period τ_e (distance between folds) vs r_r for $\varepsilon_r = 50$.
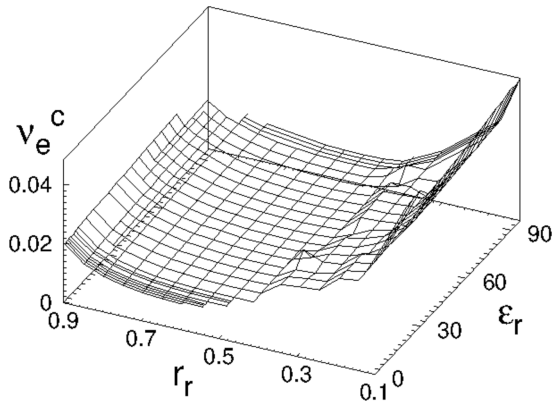
but also, to a lesser degree, other frequencies contribute to the assembly of the structure. To consider all the contributions, we calculate the center of frequencies (ν_e^c) and the dispersion ($\delta\nu_e$) around it, considering the spectral function as the weight factor for each frequency. In Fig. 15 we show curves of the spectral function for three typical cases. In the first place, we note a dominant frequency peak, which, we corroborate, coincides with the inverse of the distance between folds of the localized patterns. When comparing them, we note that the frequency peaks in cases (a) and (b), although very low, occupy a wider band than the other case (c), but which shows peak heights comparable to that of the main one. Then we notice that the frequency peaks of cases (b) and (c) are closer together than those of the first one (a). Both the center of frequency and the dispersion reflect the difference between case (b) and the other two, the adopting latter larger values than for case (b). This is due to the fact that while in cases (a) and (c) the differences between the separation between peaks (greater in one case than the other) and their height (less in one case than the other) mutually compensate their effect on dispersion and center of frequencies, such compensation does not happen for case (b). Figures 16, 17, and 18 show the surfaces $\tau_e(r_r, \varepsilon_r)$, $\nu_e^c(r_r, \varepsilon_r)$, and $\delta\nu_e(r_r, \varepsilon_r)$. We observe that the spatial period of the pattern (τ_e) is monotonically increasing with both the reach and the intensity of the repulsive forces. However, τ_e is considerably more sensitive with r_r than
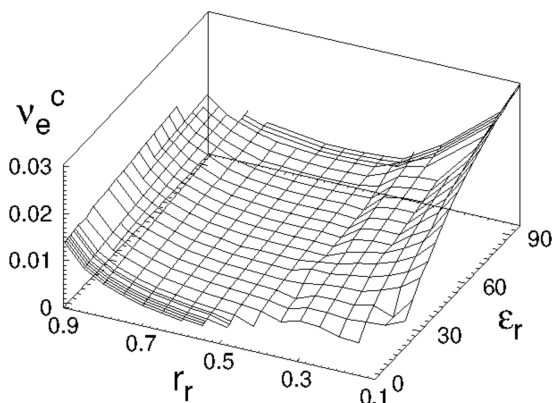
with ε_r. On the other hand, the other two surfaces (Figs. 17 and 18) present a "valley" in the central region of values of r_r. In the "valley," the spectral function is as shown in Fig. 15(b) and identified as case (b). Case (a) is typical of the "hillside" corresponding to the smallest r_r values, and case (c) is characteristic of the "hillside" corresponding to the largest r_r values. Looking at the three figures it is clear that r_r impacts the frequency spectrum much more than ε_r. In general, all three surfaces are smooth except for a few breaks in the range of r_r: [0.25–0.55]. To observe this phenomenon in more detail, in Fig. 19, 20, and 21 we show the curves corresponding to a given intensity value ($\varepsilon_r = 50$). We observe that such behavior is a reflection of somewhat abrupt changes in the shape of the structures. The latter is illustrated in Fig. 22, which shows three stationary structures, which emerge as r_r changes in the range of reference values. Beyond the aforementioned range, the width of the emerging structures increases with the reach of repulsive forces but without changing the general shape of the pattern envelope. The fourth structure shown in Fig. 22 exemplifies this situation. For smaller values of the intensity something similar happens, but the forms that the envelope of the pattern takes within the break range are different. Figure 23 illustrates these differences.
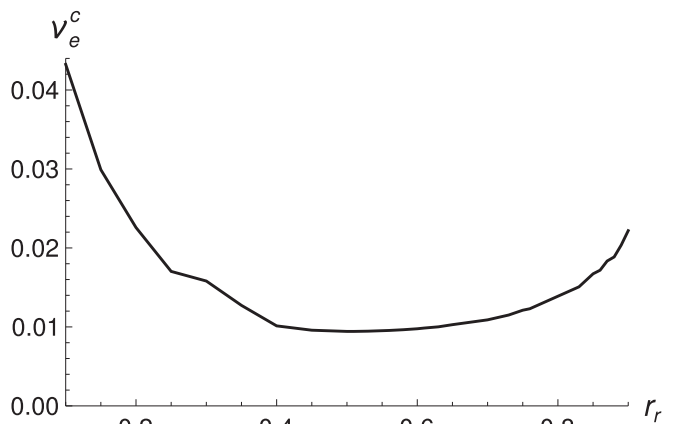

FIG. 18. Dispersion ($\delta\nu_e$) vs r_r and ε_r.

FIG. 20. Center of frequencies (ν_e^c) vs r_r for $\varepsilon_r = 50$.
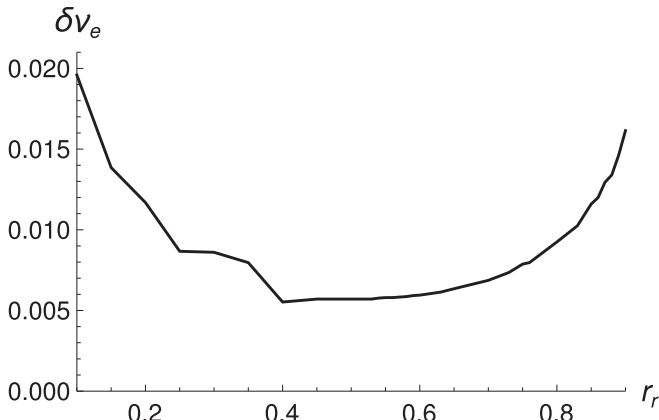
FIG. 21. Dispersion (δv_e) vs r_r for $\varepsilon_r = 50$.

If we consider a linear world, increasing the width of a localized structure is a defense against predators, since it increases the number of unexposed individuals (only individuals located at the limits of the structure are exposed). In the same sense, given a mass of individuals, a single structure is more convenient than several small ones. However, the surface exposed to food is small, since it can enter only through the limit points of the structure. A patterned structure solves the problem, since the surface exposed to food is strongly increased, while the attack of predators is circumscribed only to the limits of the structure. We observed that the relevant parameter that considers both requirements (access to food and defense against predators) is the width of the structure (localized pattern) multiplied by the spatial frequency, that is, the number of folds that make up the structure. We conclude that the more folds, the more surface exposed to food in relation to the surface exposed to predators. Figures 24 and 25 show the corresponding surfaces: the width of the structure (SW) and the number of folds (FN) as a function of r_r and ε_r. We observe that the width of the structure is monotonically increasing with both control parameters, although it is clear

FIG. 22. Localized patterns for $\varepsilon_r = 50$. In the break range (a) $r_r = 0.3$, (b) $r_r = 0.4$, and (c) $r_r = 0.5$. Beyond break range (d) $r_r = 0.8$.
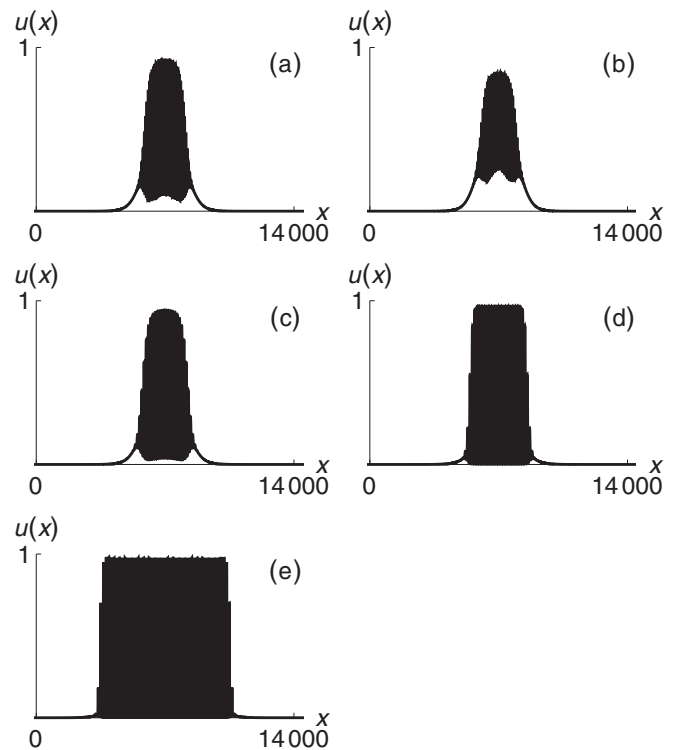

FIG. 23. Localized patterns for $\varepsilon_r = 15$. In the break range (a) $r_r = 0.3$, (b) $r_r = 0.4$, (c) $r_r = 0.45$, and (d) $r_r = 0.55$. Beyond break range (e) $r_r = 0.8$.

that the relevant parameter is r_r. We also notice that the slope is much larger above the break range. On the other hand, the surface corresponding to the number of folds has a "valley." The "hillside" due to smaller r_r values is justified by short periods (high density of folds) and the other "hillside," because the structures that emerge are very wide. They are two different strategies that serve to optimize the combination of both objectives: access to food and defense against predators.
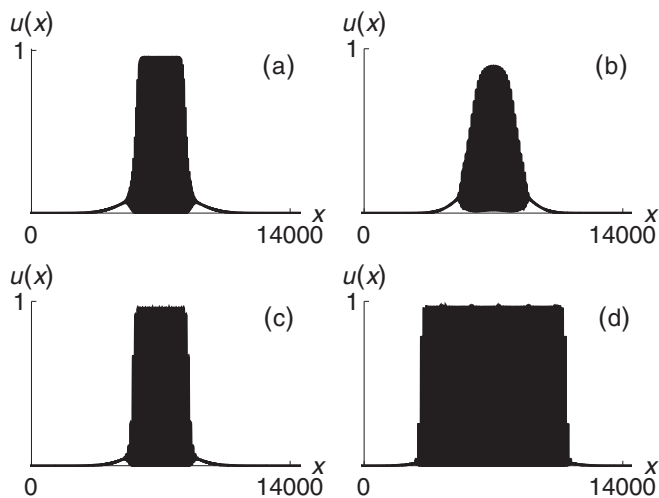
B. Cyclical and chaotic cases

Although we consider that the views of Fig. 5, 8, and 10 are sufficient evidence to characterize the respective cyclical and chaotic behaviors reported, the Fourier transform of the
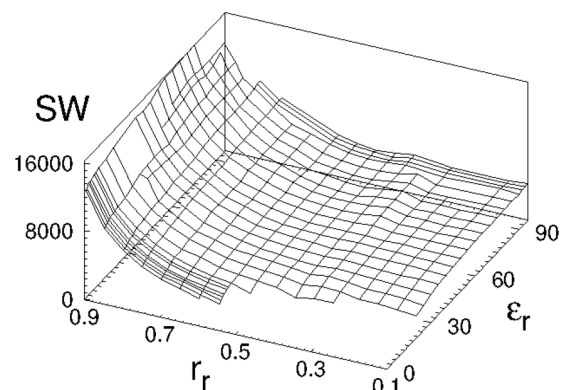

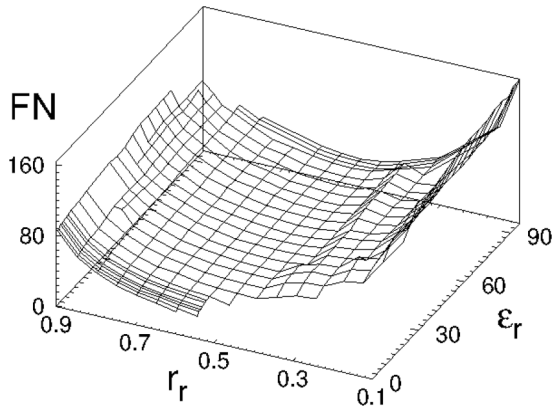FIG. 24. Width of the localized pattern (SW) vs r_r and ε_r.

FIG. 25. Number of folds of localized pattern (FN) vs r_r and ε_r.

evolution of the linear response parameter is a way of objectifying such characterization.

In Figs. 26 and 27 we show the spectral function corresponding to the periodic cases shown in Fig. 5(a) and Fig. 8. We note that only a few specific frequencies contribute to the $\alpha(t)$ curve. As expected, for both cases, the inverse of the frequency corresponding to the dominant peak coincides with the period of the corresponding curve. In Figs. 28 and 29 we show the spectral function corresponding to the chaotic cases shown in Fig. 5(b) and Fig. 10. We note that for both cases, typical of chaotic situations, an infinity of frequencies contribute to characterize the $\alpha(t)$ curve.

VI. BRIEF CONCLUSIONS

The life of large groups of individuals is governed by links and rules of a diverse nature which can be translated into complex physical interactions. Although mesoscopic models resort to a simplification of such interactions, they are able to predict global aspects of their behavior. In this regard, researchers on the subject agree on the relevance of attractive and repulsive forces among the individuals that make up these groups. We have found a simple way to characterize the impact of attractive and repulsive interaction forces on a set of individuals that holds their number around an optimal
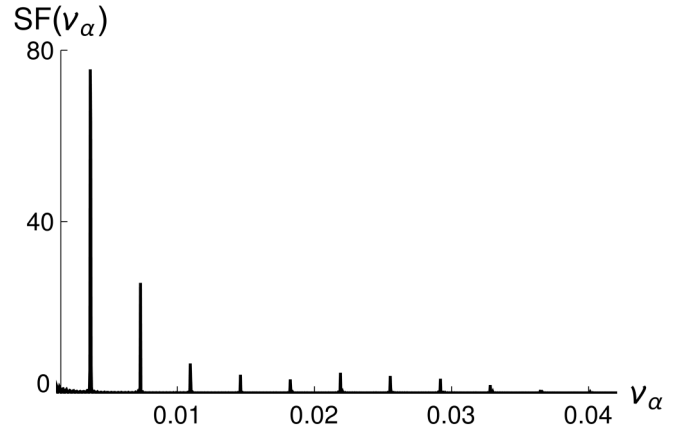

FIG. 27. Spectral function (SF) corresponding to $\alpha(t)$ curve for a periodic abnormal case: $r_r = 0.63$ and $\varepsilon_r = 4$.

value. We have been surprised by the great diversity of stable solutions that can be found just by varying the reach and intensity of the repulsive forces. Within that diversity we find multistability: many possible answers for a given set of values that characterize the system and that we call a response state. Although it still surprises us, it is currently expected for a set of self-assembled individuals, the interactions between individuals act on scales much smaller than the size of the structures found. However, in this work, such scales appear in the spatial period of the localized patterns, as well as in the "fingers" of abnormal structures.

Our view is that given a disturbance of the environment, the set of individuals "read" their inherent order, and depending on it, decide a response state (which is defined by the set of values that characterize the system state, among which the reach and intensity of the repulsive forces are included) and an initial profile. Thus, if the response state is multistable, the initial profile defines the definitive answer.

We have focused on the solutions we call normal. In particular, folds in localized patterns can be associated with the wrinkles and rings observed in biofilms. In this regard, we have explained how the number of folds impacts the relationship access to food and defense against predators.
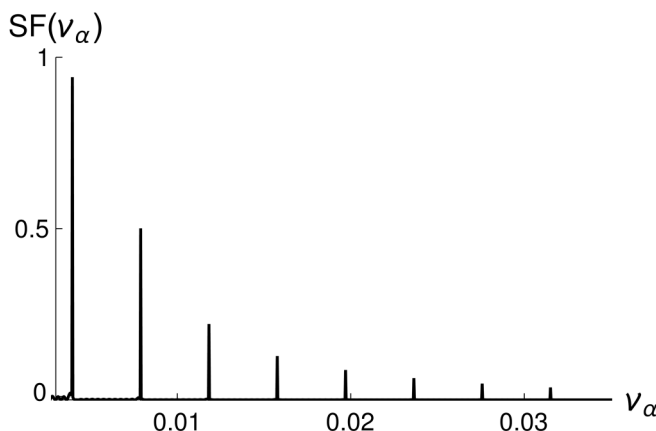

FIG. 26. Spectral function (SF) corresponding to $\alpha(t)$ curve for a periodic normal case: $r_r = 0.4$ and $\varepsilon_r = 90$.
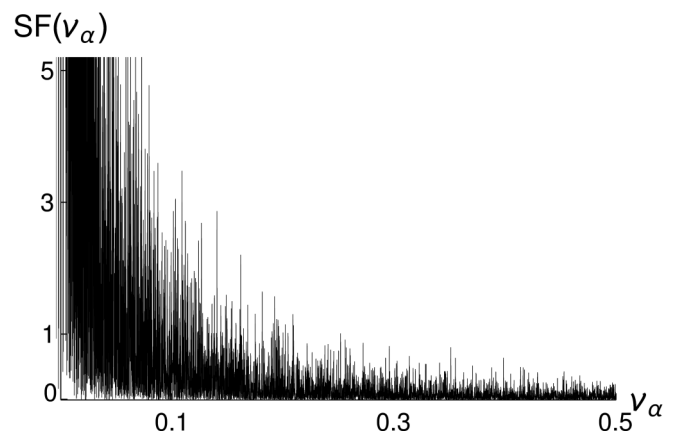

FIG. 28. Spectral function (SF) corresponding to $\alpha(t)$ curve for a chaotic normal case: $r_r = 0.35$ and $\varepsilon_r = 60$.
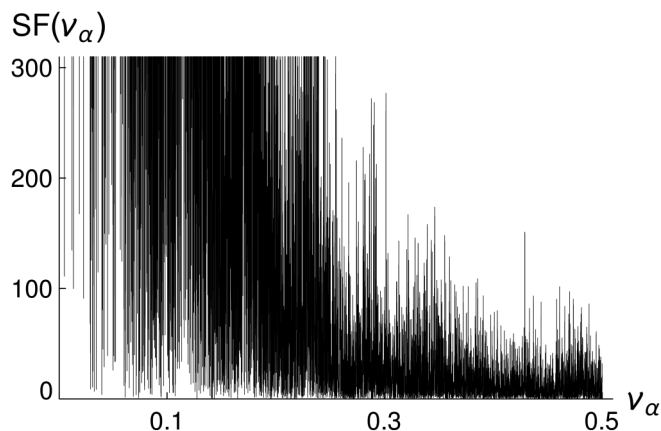
SF(ν_α)

FIG. 29. Spectral function (SF) corresponding to $\alpha(t)$ curve for a chaotic abnormal case: $r_r = 0.35$ and $\varepsilon_r = 19$.

Finally, we mentioned that, among the different solutions, we find pairs of asymmetrical-antisymmetric structures that move in opposite directions and whose speed increases with asymmetry. This result draws our attention, not only for the fact itself, but also because the edge conditions of the system impose zero current. However, far from the edges, such currents are not prohibited. We intuit that the observed asymmetries are stabilized by these same currents. This phenomenon is consistent with the fact that for the cyclic or chaotic cases, the structures asymmetry changes with time and therefore, also, the direction of their speed. Furthermore, dynamic solutions can be associated with a reconversion game in which asymmetries in densities and currents feed off each other to give rise to that kind of "dance" that structures perform. Of course, this is an issue that requires extra work that we leave for the near future.

[1] M. Hildebrand and A. S. Mikhailov, Mesoscopic modeling in the kinetic theory of adsorbates, J. Phys. Chem. **100**, 19089 (1996).

[2] M. Hildebrand, A. S. Mikhailov, and G. Erlt, Nonequilibrium stationary microstructures in surface chemical reactions, Phys. Rev. E **58**, 5483 (1998).

[3] S. E. Mangioni, Nano-pattern stabilization by multiplicative noise, Physica A **389**, 1799 (2010).

[4] S. E. Mangioni, A mechanism for pattern formation in dynamic populations by the effect of gregarious instinct, Physica A **391**, 113 (2012).

[5] S. Mangioni, Extinction avoidance by aggregation in excitable kinetics, Eur. Phys. J. B **86**, 390 (2013).

[6] S. Mangioni, Interaction between "dissipative solitons" stabilized by aggregation in excitable kinetics, Eur. Phys. J. B **87**, 248 (2014).

[7] M. G. Clerc, D. Escaff, and V. M. Kenkre, Patterns and localized structures in population dynamics, Phys. Rev. E **72**, 056217 (2005).

[8] M. G. Clerc, D. Escaff, and V. M. Kenkre, Analytical studies of fronts, colonies, and patterns: Combination of the Allee effect and nonlocal competition interactions, Phys. Rev. E **82**, 036210 (2010).

[9] K. J. Painter, J. M. Bloomfield, J. A. Sherratt, and A. Gerisch, A nonlocal model for contact attraction and repulsion in heterogeneous cell populations, Bull. Math. Biol. **77**, 1132 (2015).

[10] M. Banerjee and V. Volpert, Spatio-temporal pattern formation in Rosenzweig-MacArthur model: Effect of nonlocal interactions, Ecol. Complex. **30**, 2 (2017).

[11] R. D. Alexander, The evolution of social behavior, Ann. Rev. Ecol. Syst. **5**, 325 (1974).

[12] G. D. Ruxton and T. N. Sherratt, Aggregation, defence and warning signals: The evolutionary relationship, Proc. R. Soc. B **273**, 2417 (2006).

[13] U. Lopez, J. Gautrais, I. D. Couzin, and G. Theraulaz, From behavioural analyses to models of collective motion in fish schools, Interface Focus **2**, 693 (2012).

[14] A. Huth and C. Wisse, The simulation of fish schools in comparison with experimental data, Ecol. Modell. **75/76**, 135 (1994).

[15] I. Aoki, A simulation study on the schooling mechanism in fish, Bull. Jpn. Soc. Sci. Fish **48**, 1081 (1982).

[16] I. Aoki, An analysis of the schooling behavior of fish: Internal organization and communication process, Bull. Ocean. Res. Inst. Univ. Tokyo **12**, 1 (1980).

[17] Y. Inada and K. Kawachi, Order and flexibility in the motion of fish schools, J. Theor. Biol. **214**, 371 (2002).

[18] D. E. O. Juanico, Self-organized pattern formation in a diverse attractive-repulsive swarm, Europhys. Lett. **86**, 48004 (2009).

[19] D. Morale, V. Capasso, and K. Oelschlager, An interacting particle system modelling aggregation behavior: From individuals to populations, J. Math. Biol. **50**, 49 (2005).

[20] H. Poysa, J. Rintala, D. H. Johnson, J. Kauppinen, E. Lammi, T. D. Nudds, and V. M. Vaananen, Environmental variability and population dynamics, Ecol. Evol. **6**, 7004 (2016).

[21] B. E. Sæther, V. Grøtan, S. Engen, T. Coulson, P. R. Grant, M. E. Visser, J. E. Brommer, B. R. Grant, L. Gustafsson, B. J. Hatchwell, K. Jerstad, P. Karell, H. Pietiainen, A. Roulin, O. W. Røstad, and H. Weimerskirch, Demographic routes to variability and regulation in bird populations, Nat. Commun. **7**, 12001 (2016).

[22] D. Papageorgiou and D. R. Farine, Group size and composition influence collective movement in a highly social terrestrial bird, eLife **9**, e59902 (2020).

[23] J. D. Murray, *Mathematical Biology* (Springer, New York, 1993).

[24] S. E. Mangioni and H. S. Wio, Interplay between noise and boundary conditions in pattern formation in adsorbed substances, Phys. Rev. E **71**, 056203 (2005).

[25] D. Karaboga and B. Basturk, A powerful and efficient algorithm for numerical function optimization: Artificial bee colony (ABC) algorithm, J. Global Optim. **39**, 459 (2007).

[26] K. M. Passino, *Biomimicry for Optimization, Control, and Automation* (Springer-Verlag, London, 2005).

[27] M. J. Mataric, Minimizing complexity in controlling a mobile robot population, in *Proc. 1992 IEEE Intl. Conf. on Robotics and Automation, Nice, France* (1992), Vol. 1, pp. 830–835.

[28] H. Dalton, A. Goodman, and K. Marshall, Diversity in surface colonization behavior in marine bacteria, J. Ind. Microbiol. **17**, 228 (1996).

[29] L. Hall-Stoodley, J. Costerton, and P. Stoodley, Bacterial biofilms: From the natural environment to infectious diseases, Nat. Rev. Microbiol. **2**, 95 (2004).

[30] J. K. Teschler, D. Zamorano-Sánchez, A. S. Utada, C. J. Warner, G. C. Wong, R. G. Linington, and F. H. Yildiz, Living in the matrix: Assembly and control of *Vibrio cholerae* biofilms, Nat. Rev. Microbiol. **13**, 255 (2015).

[31] H.-C. Flemming, J. Wingender, U. Szewzyk, P. Steinberg, S. A. Rice, and S. Kjelleberg, Biofilms: An emergent form of bacterial life, Nat. Rev. Microbiol **14**, 563 (2016).

[32] B. C. R. Bertram, Living in groups: Predators and prey, in *Behavioral Ecology*, edited by J. R. Krebs and N. B. Davies (Blackwell, Oxford, 1978), pp. 64–96.

[33] A. R. E. Sinclair, Does interspecific competition or predation shape the African ungulate community? J. Anim. Ecol. **54**, 899 (1974).

[34] R. W. Wrangham and D. I. Rubenstein, Social evolution in birds and mammals, in *Ecological Aspects of Social Evolution*, edited by D. I. Rubenstein and R. W. Wrangham (Princeton University Press, Princeton, 1986), pp. 452–470.

[35] D. M. Gordon, The ecology of collective behavior in ants, Annu. Rev. Entomology **64**, 35 (2019).

[36] B. Sillen-Tullberg and O. Leimar, The evolution of gregariousness in distasteful insects as a defense against predators, Am. Nat. **132**, 723 (1988).

[37] J. L. Deneubourg, A. Lioni, and C. Detrain, Dynamics of aggregation and emergence of cooperation, Biol. Bull. **202**, 262 (2002).

[38] S. Depickére, D. Fresneau, and J.-L. Deneubourg, A basis for spatial and social patterns in ant species: Dynamics and mechanisms of aggregation, J. Insect Behav. **17**, 81 (2004).

[39] R. Eastwood, Successive replacement of tending ant species at aggregations of scale insects (Hemiptera: Margarodidae and Eriococcidae) on *Eucalyptus* in south-east Queensland, Aust. J. Entomol. **43**, 1 (2004).

[40] A. F. Hunter, Gregariousness and repellent defences in the survival of phytophagous insects, OIKOS **91**, 213 (2000).

[41] D. R. Farine, L. M. Aplin, C. J. Garroway, R. P. Mann, and B. C. Sheldon, Collective decision making and social interaction rules in mixed-species flocks of songbirds, Anim. Behav. **95**, 173 (2014).

[42] M. Boraas, D. Seale, and J. Boxhorn, Phagotrophy by a flagellate selects for colonial prey: A possible origin of multicellularity, Evol. Ecol. **12**, 153 (1998).

[43] K. Sauer, A. K. Camper, G. D. Ehrlich, J. W. Costerton, and D. G. Davies, *Pseudomonas aeruginosa* displays multiple phenotypes during development as a biofilm, J. Bacteriol. **184**, 1140 (2002).

[44] E. W. Rice, C. J. Johnson, R. M. Clark, K. R. Fox, D. J. Reasoner, M. E. Dunnigan, P. Panigrahi, J. A. Johnson, and J. G. Morris Jr., Chlorine and survival of "rugose" Vibrio cholerae, Lancet **340**, 740 (1992).

[45] C. Matz, D. McDougald, A. Moreno, P. Yung, F. H. Yildiz, and S. Kjelleberg, Biofilm formation and phenotypic variation enhance predation-driven persistence of Vibrio cholerae, Proc. Natl. Acad. Sci. USA **102**, 16819 (2005).

[46] S. Beyhan and F. H. Yildi, Smooth to rugose phase variation in *Vibrio cholerae* can be mediated by a single nucleotide change that targets c-di-GMP signalling pathway, Mol. Microbiol. **63**, 995 (2007).

[47] P. S. Stewart and M. J. Franklin, Physiological heterogeneity in biofilms, Nat. Rev. Microbiol. **6**, 199 (2008).

[48] K. T. Schiessl, F. Hu, J. Jo, S. Z. Nazia, B. Wang, A. Price-Whelan, W. Min, and L. E. P. Dietrich, Phenazine production promotes antibiotic tolerance and metabolic heterogeneity in *Pseudomonas aeruginosa* biofilms, Nat. Commun. **10**, 762 (2019).

[49] F. Bocci, Y. Suzuki, M. Lu, and J. N. Onuchic, Role of metabolic spatiotemporal dynamics in regulating biofilm colony expansion, Proc. Natl. Acad. Sci. USA **115**, 4288 (2018).

[50] A. Czirók, E. Ben-Jacob, and T. Vicsek, Formation of complex bacterial colonies via self-generated vortices, Phys. Rev. E **54**, 1791 (1996).

[51] P. Thomen, J. D. P. Valentin, A.-F. Bitbol, and N. Henry, Spatiotemporal pattern formation in *E. coli* biofilms explained by a simple physical energy balance, Soft Matter **16**, 494 (2020).

[52] J. B. Xavier, E. Martinez-Garcia, and K. R. Foster, Social evolution of spatial patterns in bacterial biofilms: When conflict drives disorder, Am. Nat. **174**, 1 (2009).

[53] D. O. Serra, A. M. Richter, F. Mika, and R. Hengge, Cellulose as an architectural element in spatially structured *Escherichia coli* biofilms, J. Bacteriol. **195**, 5540 (2013).

[54] L. E. P. Dietrich, C. Okegbe, A. Price-Whelan, H. Sakhtah, R. C. Hunter, and D. K. Newmana, Bacterial community morphogenesis is intimately linked to the intracellular redox state, J. Bacteriol. **195**, 1371 (2013).

[55] D. O. Serra, A. M. Richter, G. Klauck, F. Mika, and R. Hengge, Microanatomy at cellular resolution and spatial order of physiological differentiation in a bacterial biofilm, mBio **4**, e00103 (2013).

[56] J. Yan, C. D. Nadell, H. A. Stone, N. S. Wingreen, and B. L. Bassler, Extracellular-matrix-mediated osmotic pressure drives *Vibrio cholerae* biofilm expansion and cheater exclusion, Nat. Commun. **8**, 327 (2017).

[57] C. Fei, S. Mao, J. Yan, R. Alert, H. A. Stone, B. L. Bassler, N. S. Wingreen, and A. Kosmrlj, Nonuniform growth and surface friction determine bacterial biofilm morphology on soft substrates, Proc. Natl. Acad. Sci. USA **117**, 7622 (2020).

[58] R. M. Harshey, Bacterial motility on a surface: Many ways to a common goal, Annu. Rev. Microbiol. **57**, 249 (2003).

[59] W. H. Press, S. A. Teukolsky, W. T. Vetterling, and B. P. Flannery, *Numerical Recipes in FORTRAN 77: Volume 1 of Fortran Numerical Recipes: The Art of Scientific Computing: Fortran Numerical Recipes* (Cambridge University Press, Cambridge, 1997).